Evolution of gas diffusion layer structures for aligned Pt nanowire electrodes in PEMFC applications

Lu, Yaxiang; Steinberger-Wilckens, Robert; Du, Shangfeng

DOI:
10.1016/j.electacta.2018.05.008

Document Version
Peer reviewed version

Citation for published version (Harvard):
Lu, Y, Steinberger-Wilckens, R & Du, S 2018, 'Evolution of gas diffusion layer structures for aligned Pt nanowire electrodes in PEMFC applications', *Electrochimica Acta*, vol. 279, pp. 99-107.
https://doi.org/10.1016/j.electacta.2018.05.008

Accepted Manuscript

Evolution of gas diffusion layer structures for aligned Pt nanowire electrodes in PEMFC applications

Yaxiang Lu, Robert Steinberger-Wilckens, Shangfeng Du

PII: S0013-4686(18)31012-0

DOI: 10.1016/j.electacta.2018.05.008

Reference: EA 31794

To appear in: *Electrochimica Acta*

Received Date: 23 November 2017

Revised Date: 23 April 2018

Accepted Date: 1 May 2018

Please cite this article as: Y. Lu, R. Steinberger-Wilckens, S. Du, Evolution of gas diffusion layer structures for aligned Pt nanowire electrodes in PEMFC applications, *Electrochimica Acta* (2018), doi: 10.1016/j.electacta.2018.05.008.

Evolution of Gas Diffusion Layer Structures for Aligned Pt Nanowire Electrodes in PEMFC applications

Yaxiang Lu,[1,2] *Robert Steinberger-Wilckens and Shangfeng Du*[1]*

[1] School of Chemical Engineering, University of Birmingham, Edgbaston, Birmingham B15 2TT, UK

[2] Key Laboratory for Renewable Energy, Beijing Key Laboratory for New Energy Materials and Devices, Beijing National Laboratory for Condensed Matter Physics, Institute of Physics, Chinese Academy of Sciences, Beijing 100190, China.

E-mail: s.du@bham.ac.uk

Abstract:

Gas diffusion layer (GDL), consisting of a microporous layer (MPL) and a carbon fibre substrate, is one of the major components in proton exchange membrane fuel cells (PEMFCs). In gas diffusion electrodes (GDEs) with in-situ grown aligned Pt nanowire (NW) catalysts, the GDL can also provide an important function in controlling the growth and distribution of the Pt nanowires. In this work, a systematic investigation is conducted to evaluate the evolution of the GDL structure on the PtNW growth process to prepare GDEs. The influence mechanisms including carbon loading, carbon composition and polytetrafluoroethylene (PTFE) loading in the MPL and PTFE in the carbon fibre substrate on the electrode power performance are studied in detail. An optimum structure for MPL, 4 mg cm^{-2} carbon loading with an equal amount of carbon black (CB) and acetylene black (AB), plus 5% PTFE loading, is deserved. This GDL structure can provide suitable substrate coverage, reasonable surface nucleation sites and required hydrophobicity for the in-situ growth of PtNWs. The results indicate that the GDL features play a significant role in the growth and distribution of the obtained Pt nanowires to achieve high performance GDEs for PEMFC application.

Keywords: Gas diffusion layer; Microporous layer; Pt; nanowire; Proton exchange membrane fuel cell (PEMFC)

1. Introduction

Gas diffusion layer (GDL) is one of the key components in proton exchange membrane fuel cells (PEMFCs). It usually consists of double functional layers: one is a macroporous substrate layer and the other is a microporous layer (MPL) coated on the surface of the substrate.[1-3] The substrate is usually made from porous stacked carbon fibres and treated by a water-proofing agent such as polytetrafluoroethylene (PTFE).[4-6] The MPL is made from carbon nanospheres for an excellent electrical conductivity and a hydrophobic polymeric binder, i.e. PTFE to maintain the integrity of carbon nanospheres and facilitate an efficient water transport out of the catalyst layers (CLs).[7-9] Therefore, the whole GDL is believed to provide mechanical strength to support CLs, deliver reactants to and remove produced water from CLs as well as reduce interfacial contact resistance (ICR) with CLs.[10-12]

With a high specific surface area (ca. 250 $m^2 g^{-1}$),[13] Vulcan XC-72R carbon black (CB) is extensively used to fabricate MPLs in commercial GDLs and also as catalyst supports.[14] Acetylene black (AB), with a surface area ranged in 15-70 $m^2 g^{-1}$, is also commonly used in MPLs to achieve a homogeneous surface.[15] The mixture of CB and AB with various compositions can be used to control the surface properties of MPLs such as specific surface area, porosity and electrical conductivity. In addition, PTFE as the additive agent in both the substrate and MPL to avoid water flooding, can also significantly affect the surface wettability and porosity, further influencing the structure of GDLs.[16]

As a component next to the CL in fuel cell construction, the characteristics of the GDL considerably affect the performance of PEMFCs, especially when the gas diffusion electrode (GDE) technique is employed by directly coating catalysts on the GDL surface.[17, 18] Different from the conventional methods by painting[19, 20], spraying[21, 22] or printing[23,

24] the catalyst layer onto the GDL surface, our group have developed aligned Pt nanowire (NW) GDE concept by in-situ growing Pt nanowires on the GDL surface.[25-27] The achieved extremely thin catalyst layer consisting of only a monolayer array of single-crystal Pt NWs could effectively reduce mass transfer resistance and boost the catalyst utilisation ratio for an improved power performance.[28] However, the in-situ growth of PtNW CLs is obtained by a one-pot wet-chemical process, where the GDL structure, including the porosity, homogeneity, hydrophobicity, etc. can significantly influences the growth and distribution of the Pt NWs on the GDL surface.[28] Therefore, a systematic investigation on the evolution mechanism of the GDL structure for Pt nanowire growth is required to achieve high-performance GDEs for PEMFC applications.

In this work, the evolution of GDL structures on the performance of the aligned PtNW GDEs is studied in detail. Considering the crystal nucleation and growth processes of Pt NWs and the actual PtNW GDE performance in single PEMFCs, the carbon loading and carbon composition in the MPL, as well as the PTFE amounts in both of the substrate and MPL are investigated comprehensively. It is found that the GDEs with a proper GDL structure can exhibit an enhanced performance compared to the reported research work. The morphology and distribution of the Pt NWs on the GDL surface are discussed in detail considering the electrochemical impedance spectroscopy (EIS) analysis and single cell test results.

2. Experimental Section

2.1 Chemicals and Materials

All chemicals and materials were used as received without any further purification. Hexachloroplatinic acid hexahydrate ($H_2PtCl_6 \cdot 6H_2O$, ≥37.50% Pt basis) and PTFE (60 wt% dispersion in H_2O) were purchased from Sigma-Aldrich UK. Formic acid (CH_2O_2, 90%) and isopropanol (IPA) (C_3H_8O, >99.5%) were obtained from Fisher Scientific UK. Vulcan

XC-72R carbon black (CB) and acetylene black (AB) (100% compressed, 99.9+%) were purchased from Fuel Cell Store USA and Alfa Aesar USA, respectively. DuPont Nafion® 212 membrane and Nafion® solution (D1021, 10 wt%) were obtained from Ion Power Inc. SIGRACET® GDLs 35BA, 35BC, 35CC and 35DC carbon paper were supplied by SGL Group. The gas diffusion electrodes (ELE1065-0983, 0.4 mg_{Pt} cm^{-2}) were obtained from Johnson Matthey Fuel Cells Ltd and used as anodes for fabricating fuel cells. Ultrapure water (18.2 MΩ cm) from a Millipore water system was used throughout.

2.2 Carbon loading in MPLs

35BA, the pure carbon fibre paper without MPL, was used as the substrate for fabricating GDLs with self-painted MPLs. According to the data from SGL Group, the areal weight of 35BA is 54 g m^{-2}, and that of 35BC GDL which consists of 35BA with the standard MPL is 110 g m^{-2}. Considering there is 20% PTFE in the standard MPL (based on the total MPL weight), the calculated carbon loading is 4.48 mg cm^{-2}. This value is much higher than those reported in literature that is usually in the range of 0.5-2 mg cm^{-2}.[29-31] To find the optimal carbon amount for Pt NWs GDE, the carbon loading in MPLs was studied based on the standard 35BA with the CB loadings of 1, 3, 4, 4.48 and 5 mg cm^{-2}. The PTFE percentage in the MPL was 20% based on the total MPL weight. The mixtures of CB and PTFE were dispersed in ultrapure water and IPA solution by ultrasonic processing with bath for 15 min (U300, Ultrawave, UK) and horn for 10 min (130 W, 30% amplitude, VCX 130, SONICS, USA). The resulting carbon inks were brush painted on 35BA substrate, and dried overnight at 40 ^{o}C in the oven. After that, the GDL samples were heated at 240 ^{o}C for 30 min in air to remove the remained dispersing agent and then at 350 ^{o}C for 30 min to improve the distribution of PTFE.[9] The treated GDLs were then ready to use for the growth of Pt NWs.

2.3 Carbon composition in MPLs

With the optimized carbon loading, a carbon mixture of CB and AB were employed for the preparation of carbon inks. The percentage of CB was adjusted to 0, 10, 25, 40, 50, 60, 75, 90 and 100% in the carbon mixture. All other processes are the same as described in Section 3.2.

2.4 PTFE loading in substrates and MPLs

To study the effect of PTFE in the substrate, Sigracet® 35BC, 35CC and 35DC GDLs, all with the standard Sigracet MPL but different PTFE loadings of 5, 10 and 20% in the substrate, respectively, were used. 35BA was used as the based substrate for the fabrication of self-painted GDLs to investigate the influence of PTFE in the MPL. Self-painted MPLs were prepared with different PTFE loadings based on the optimized carbon loading and carbon composition. The PTFE loadings were 5, 10, 15, 20, 25, 30 and 40% (to total MPL weight) in carbon inks. The self-painted GDLs were then treated as mentioned above for the growth of Pt NWs.

2.5 Pt NWs GDE preparation and physical characterization

Pieces of standard and the self-painted GDLs were used as supports for Pt nanowire growth. The detailed procedure is described in our previous studies.[32,33] Before use, the GDLs were cleaned with ultrapure water and IPA. For the in-situ growth of 0.4 mg cm^{-2} Pt nanowires on a piece of 16 cm^2 GDL, 17 mg $H_2PtCl_6 \cdot 6H_2O$ (6.4 mg Pt) and 0.53 mL formic acid were added to 10.6 mL ultrapure water. The GDL was then immersed and push to the bottom in the mixed solution in a 10 cm glass Petri dish by a plastic tweezer and stored at room temperature for Pt nanowire growth. After the colour of the solution changed from yellow to colourless and the growth of nanowire was completed, the samples were rinsed using ultrapure water and IPA, followed by drying at 40 ^oC overnight. The as-prepared carbon paper samples with in-situ grown Pt nanowires were directly used as GDEs at the cathode side. The microstructure of CB and AB was characterized by a high-resolution transmission

electron microscope (HR-TEM, Philips CM200 FEG). The morphology and distribution of Pt nanowires within GDEs were analysed by a field emission scanning electron microscope (FE-SEM, JEOL 7000F, operating at 20 kV).

2.6 Membrane electrode assembly (MEA) fabrication

The commercial Johnson Matthey GDEs with a Pt nanoparticle loading at 0.4 mg_{Pt} cm^{-2} were used as anodes and the as-prepared GDEs were used as cathodes. Before being fabricated into MEAs the GDE surface was coated with a thin layer of Nafion ionomer (0.6 mg cm^{-2}). The two GDEs were then sandwiched at both sides of a 6×6 cm^2 Nafion 212 membrane and the MEA was hot pressed at 125 ^oC under 4.9 MPa pressure for 2 min.

2.7 Fuel cell tests

The fabricated MEAs were tested in a PEMFC test stand (PaxiTech-BioLogic FCT-50S) with electrochemical impedance spectroscopy (EIS) capabilities. The gasket used in fuel cell testing was PTFE sheet with a thickness of 254 µm at both cathode and anode sides. The MEAs were conditioned by a break-in at 0.6 V for 7 h, and after that polarisation curves were recorded at a scan rate of 5 mV s^{-1}. The stoichiometry for H_2 and air was 1.3/2.4 with the minimum gas flow rates of 120 and 300 mL min^{-1}, respectively. EIS measurements were performed in the frequency range from 10 kHz to 0.1 Hz with amplitudes of 0.05, 1 and 2 A. Three current densities at low, medium and high values, i.e. at 0.05, 0.5 and 1.0 A cm^{-2}, respectively, were chosen for the measurements. All the displayed resistances in the EIS spectra indicate the area specific resistance (ASR). Water flooding test based on a 24 h hold at 0.6 V was also conducted. All the above tests were conducted at 70 ^oC with gases fully humidified before entering the cell. The backpressure was 2 barg on the pressure gauge at both sides. Cathode cyclic voltammograms (CVs) were recorded using an EZstat-Pro system integrated with the test stand. The cathode was fed with fully humidified N_2 at 300 mL min^{-1}

and the anode was fed with fully humidified pure H_2 at 120 mL min^{-1}, serving as both reference and counter electrodes. Then, the cathode potential was cycled between 0.05 and 1.2 V at 20 mV s^{-1} for 5 cycles, and the fifth cycle was recorded. The cell temperature and backpressure for CVs were 25 °C and 0 barg, respectively. The electrochemical surface area (ECSA) was measured by the electrochemical hydrogen adsorption/desorption method and calculated by the equation given below:

$$ECSA(m^2/g) = \left[\frac{Q_H(C)}{210\mu C\ cm^{-2} \cdot L(mg\ cm^{-2}) \cdot A_g(cm^2)}\right] \times 10^5 \quad (1)$$

where Q_H is the hydrogen adsorption or desorption charge, L is the catalyst loading (e.g. 0.4 mg_{Pt} cm^{-2}) and A_g is the area of the GDE (e.g. 16 cm^2). Q_H = 210 μC cm^{-2} is used as the conversion factor, corresponding to the charge on a polycrystalline Pt surface covered by a monolayer of hydrogen atoms [34].

3. Results and discussion

3.1. Influence of carbon loading on MPL

Surface optical microscopy images of 35BA substrate and the GDLs with self-painted MPLs with Vulcan XC-72R CB at loadings of 1, 3, 4, 4.48 and 5 mg cm^{-2} are shown in Fig. 1. It can be seen that the plain 35BA substrate (Fig. 1a) is made of stacked carbon fibres. With the CB loading of 1 or 3 mg cm^{-2} in the MPL, the substrate is not fully covered and the bottom carbon fibres are still obvious. With a higher CB loading, better coverage is achieved on the substrate surface. There is no obvious difference between the three high CB loadings. Some cracks appear on the dried MPL, which can't be avoided although they can be minimised by a complex painting approach.

The catalytic performance of Pt NWs in-situ grown on the GDLs with various CB loading was characterised in the single fuel cell and the corresponding polarisation and power density

curves are shown in Fig. 2a. The relationships of the current density at 0.6 V and the maximum power density versus the CB loading are presented in Fig. 2b. The results of Pt NWs directly grown on the 35BA substrate without the MPL are also included for comparison. It can be seen that the use of the MPL results in a significant improvement in the fuel cell performance, which is in line with the results reported in literature.[35] Importantly, the figure shows that the performance is highly dependent on the CB loading in the MPLs. With the lower CB amount of 1 and 3 mg cm^{-2}, the performance is low, and this can be ascribed to the poor contact with the polymer electrolyte membrane due to the uneven substrate surface (Fig. 3a-d), leading to a large ICR. Furthermore, some Pt NWs may grow in the substrate rather than on the MPL surface because the large pores in the substrate enable the penetration of reaction solution. In this case, there is very little ionic conducting path between substrate and the electrolyte membrane, thus no contribution to the catalytic activity. The performance increases with growing CB loading due to the improved coverage of the substrate surface (Fig. 3e-f). At 4 mg cm^{-2}, the current density at 0.6 V reaches 0.77 A cm^{-2}. With further increase of the carbon loading, the power performance decreases, although a slightly higher maximum power density is observed when CB is 4.48 mg cm^{-2}. Given that the practical fuel cell operation voltage is usually at 0.6-0.65 V, the CB loading of 4 mg cm^{-2} was regarded as the optimal amount and used in the following work. Compared with our early results by directly growing Pt nanowires on Freudenberg H2315 I6 carbon paper [25], where also no MPL was used but a much higher power performance was obtained than that from the 35BA substrate here. This can be ascribed to the different carbon fibre type and compaction density of the two GDLs. The uncompact 35BA substrate causes much more Pt NWs to grow in the large pores within the substrate, together with the larger electric resistance of 35BA, finally resulting in a very poor performance here.

EIS measurements were conducted to help understand the effect of carbon loading on the behaviour of Pt NWs. The measurements were performed at three current densities at 0.05 (Fig. 3g), 0.5 (Fig. 3h) and 1.0 A cm^{-2} (Fig. 3i), corresponding to low, mid and high current density range, respectively. At a low current density, the impedance represented by the single semicircle is dominated by the charge transfer losses, while at a large current density, a 2^{nd} semicircle appearing at the low frequency region is mainly caused by the mass transfer losses. From Fig. 3g, it can be seen that all samples show a very similar impedance, but the samples with the low carbon loadings of 1 and 3 mg cm^{-2} exhibit a much larger ohmic resistance shown by larger start points at a high frequency, which stands for the sum of all ohmic resistances from the electrode and electrolyte, including ICR. Considering the same fuel cell construction is used for all samples except the GDE, this difference can be ascribed to the large ICR between the GDE surface and the polymer electrolyte membrane, in particular the uneven GDL surface with the uncovered carbon fibres at the low carbon loading as shown in Fig. 3d. Samples with 4, 4.48 and 5 mg cm^{-2} carbon loadings all show a similar ohmic resistance due to the even MPL surface, further confirming that the main contribution to the ohmic resistance in these samples is the ICR. This is also confirmed by EIS at larger current densities of 0.5 A cm^{-2} (Fig. 3h) and 1.0 A cm^{-2} (Fig. 3i). A slightly lower charge transfer resistance is observed for the sample with a carbon loading of 4 mg cm^{-2} and lower mass transfer resistance for the one with 4.48 mg cm^{-2} at a large current density (Fig. 3c), which is in line with polarisation curves shown in Fig. 2.

3.2. Influence of carbon composition on GPL

With the optimum carbon loading of 4 mg cm^{-2} and 20% PTFE, the carbon composition in the MPL with different carbon black (CB) and acetylene black (AB) ratios was then investigated. The in-situ performance of Pt NWs GDEs from painted GDLs with different carbon compositions in the MPLs is shown in Fig. 4 with the cases of MPLs made from pure AB and

CB. It is shown in Fig. 4a that Pt NWs GDE with pure AB in the MPL exhibits the poorest performance. With the adding of CB the performance is gradually improved and achieves the highest value with CB 50%+AB 50%. At a higher CB amount, the performance slightly declines but no big difference is observed with the CB amount between 60-100%. The change of the current density at 0.6 V and the maximum power density versus various carbon compositions shown in Fig. 4b can explain the trend well. It increases at first, and then reaches the peak at the optimum composition, finally decreases with a slight difference.

To further confirm the power performance, EIS measurements were conducted and the corresponding spectra are shown in Fig. 4c-e. It can be seen that at the low current density (Fig. 4c), the Pt NWs GDE with pure AB in the MPL shows the largest resistance while the smallest value is observed for the one with CB 50%+AB 50%. Three other GDEs show a similar impedance to each other. At the medium and high current densities (Fig. 4d and e), the change trend of the impedance with the carbon composition generally agrees with that of the polarisation curves (Fig. 4a), with the smallest charge and mass transfer resistances observed for the sample with CB 50% and AB 50% and the largest of that for the one with pure AB.

To understand the mechanism of the performance change of Pt NWs GDEs on different carbon compositions, the detailed microstructures of CB and AB were analysed by transmission electron microscope (TEM). TEM images of CB and AB presented in Fig. S1 (Supporting Information) demonstrate that CB has a spherical shape with an average diameter of ca. 50 nm (Fig. S1a-b) and AB consists of graphitic flakes with irregular shape (Fig. S1c-d). According to the literature, CB has a microporous structure and thus a large specific surface area[36] while the smooth and inert surface of AB results in a lower specific surface.[37] In this work, the irregular surface of CB particles can provide more nucleation sites for Pt than the smooth AB surface. The mixture of CB and AB with different compositions may change

the external surface and internal pore structure in the MPL, influencing the growth and distribution of Pt NWs on the GDL surface. Scanning electron microscope (SEM) images of Pt NWs grown on the self-painted MPLs with different carbon compositions can further explain the performance difference and the results are shown in Fig. 4f-h. It can be seen that Pt NWs are sparsely distributed on the surface of the MPL with pure AB due to the inert surface (Fig. 4f). When 50% CB+50% AB were mixed for the carbon ink, the surface becomes preferable for Pt nanowire growth as more of them are observed on the surface and distribute uniformly with little aggregation (Fig. 4g). But when pure CB is used, the number of Pt NWs on the surface decreases and some of them even grow into the carbon surface in the pores (Fig. 4h) due to the large amount of nucleation sites on the active CB surface.

The possible reason for the different behaviour of Pt NWs on the MPL surface can be assumed in the following. When the pure AB is used, the inert surface provides few sites for the nucleation of Pt thus sparsely distributed Pt nanowire agglomerates are formed. With the increase of the CB amount, more nucleation sites are provided for more Pt NWs growth, thus a better distribution is obtained and achieves the highest performance at the optimum composition. Further increasing the CB amount results in a much loose MPL and some Pt NWs may grow into the internal surface of the pore in MPL, which has very little contribution to the power performance as there is not enough ionic conduct path to the polymer electrolyte membrane, resulting in a lower catalyst utilisation. Therefore, the carbon composition in the MPL can influence the growth of Pt NWs and further affects the fuel cell performance.

3.3. Influence of PTFE Loading on GPL

To avoid water flooding in fuel cell operation, both the substrate and MPL are usually treated with PTFE to achieve super-hydrophobicity. This feature will significantly affect the GDL porosity and the surface wettability as well. As Pt NWs GDEs are fabricated by in-situ growth

Pt NWs on the GDL surface through a wet-chemical process, the hydrophobicity feature of the GDL could affect the nucleation and growth of Pt NWs, inevitably influencing the final PEMFC performance. Therefore, the effects of the PTFE loading in both of the substrates and MPL are also investigated and the detailed information of the standard and self-painted GDLs used for the PTFE study is listed in Table 1. The EIS results of Pt NWs GDEs with various PTFE loadings in the carbon fibre substrate of GDLs at the current densities of 0.05, 0.5 and 1.0 A cm^{-2} show similar diameters of semicircles in Fig. S2, indicating that the charge and mass transfer resistances are nearly the same at three situations. Therefore, it can be concluded that the PTFE amount in the substrate shows little effect on the growth of Pt NWs.

To evaluate the effect of the PTFE loading in the MPL, GDLs with different PTFE amounts in the MPL but with the same substrate were studied. As this kind of GDLs couldn't be obtained commercially, MPLs were self-painted on 35BA substrates in the lab. Based on the optimal carbon loading of 4 mg cm^{-2} and the composition of CB 50%+AB 50%, carbon inks were prepared with different PTFE loadings of 5, 10, 15, 20, 25, 30 and 40% with respect to the total MPL weight. Fig. 5 shows the performance of Pt NWs GDEs grown on the painted MPLs with various PTFE loadings from 5 to 40%. The electrode performance generally decreases with the increase in PTFE amount. EIS measurements were conducted to further confirm the results, and a similar trend is observed to that of the polarisation curves. It shows clearly in Fig. 6a-c that at all three current density points, the sample with 5% PTFE exhibits the smallest semicircles, indicating the smallest charge and mass transfer resistances. On one hand, this can be attributed to the uniform distribution of Pt NWs on the carbon surface at low PTFE loading and the increasing agglomeration at higher PTFE amounts. On the other hand, at a high PTFE loading, the polymer in the pores partially reduces the porosity of the MPL, resulting in a large mass transfer loss.[38] To confirm the assumption for the change of the performance, the morphology and distribution of Pt NWs grown on the GDLs with the

self-painted MPLs with 5, 20 and 40% PTFE, corresponding to the low, medium and high PTFE amount, were analysed by SEM and the images are shown in Fig. 5. For the GDL with the low PTFE loading of 5% in the MPL (Fig. 6d), Pt NWs uniformly distributed on the surface and the nanowire morphology can be observed from the high magnification image. At the medium and high PTFE amount of 20% (Fig. 6e) and 40% (Fig. 6f), the distribution of Pt NWs becomes non-uniform and tends to aggregate to form superstructures, and some parts of the surface are not covered by Pt nanowires. This is because the high PTFE loading covers more surface area of the GDL thus presents a hurdle for the surface nucleation and finally leading to a dense agglomeration and non-uniform distribution. Therefore, the performance declines with the increase of the PTFE loading in the MPL.

Cathode CVs were recorded in the single cell to compare the ECSA of the Pt NWs GDEs with different PTFE loadings in MPLs. According to CV curves in 7a and the Pt precursor, the calculated ECSAs for Pt NWs GDEs with the PTFE loading of 5, 10, 15, 20, 25, 30 and 40% are 19.65, 19.35, 18.25, 18.17, 18.61, 18.25, 16.13 $m^2\ g^{-1}$, respectively. A summary of the ECSAs with the PTFE loading is shown in Fig. 7b. It can be seen that the ECSA value slowly decreases with increase in PTFE amount, but the values are still very close to each other except the value of 40% which is slightly lower. Considering the SEM analysis results (Fig. 6), it can be concluded that with the increase in PTFE amount, the catalyst utilisation slowly becomes poorer and thus a smaller ECSA value is obtained, finally resulting in an increased charge transfer loss and a lower catalytic activity (Fig. 5).

The above test results demonstrate the influence of the amount of PTFE in the MPL on the in-situ performance. To further check the possible role in water flooding during the fuel cell testing, in particular at a lower PTFE loading, e.g. 5%, Pt NWs GDEs with the painted MPLs at low, medium and high PTFE amounts were tested as cathodes by soaking at 0.6 V over a

period of ca. 24 h. Fig. 8 indicates that during this period the performance of Pt NWs GDEs is generally stable for the MPLs with low and medium PTFE loadings, but an obvious decrease can be observed with the PTFE loading of 40%. Although further investigation is needed to clarify the mechanism, one possible reason is that the high PTFE loading results in limited nucleation sites with agglomerated Pt NWs on the surface, resulting in a fast interface degradation in the operation. Hence, it can be deduced that a PTFE loading below 20% in the MPL doesn't result in water flooding in the continuous operation of fuel cells.

Furthermore, the comparison of the cathode performance of the in-situ growth of Pt NWs GDEs on Freudenberg H2315 I6 GDL carbon paper (Pt loading 0.4 mg cm^{-2}), E-TEK ELAT® GDEs LT120EW (Pt loading 0.5 mg cm^{-2}), Pt/C (20 wt%) nanoparticle GDEs, and the optimized in-situ growth Pt NWs GDEs in this work was studied (Fig. 9)[4-6] It can be seen that optimized in-situ growth Pt NWs GDEs in this work exhibits a higher power performance than the other GDEs at 0.6 V, while at the high voltage region (>0.7 V), it also presents a higher power performance. The optimum structure of in-situ growth Pt NWs GDEs in this work, 4 mg cm^{-2} carbon loading with the composition of 50% carbon black (CB) + 50% acetylene black (AB) and the 5% PTFE loading, can provide a suitable substrate coverage, reasonable surface nucleation sites and satisfying hydrophobicity for the growth of Pt NWs. Therefore a better performance is obtained compared to the in-situ growth of Pt NWs GDEs on the commercial Freudenberg H2315 I6 GDL carbon paper.[4-6]

4. Conclusion

In this study, the GDL structures such as carbon loading, carbon composition and PTFE loading were systematically investigated to understand the effects on the power performance of Pt NWs GDEs. The results demonstrate that, to achieve a high performance GDE, it is critical to control the amount of nucleation sites on the MPL surface for the production of

uniform Pt NWs with a balanced mass transport loss, but the PTFE loading in the substrate exhibited very limited influence. The obtained optimum carbon loading in the MPL is 4 mg cm^{-2}, as a higher carbon loading results in a very thick MPL and a smaller carbon amount could not cover the surface very effectively. Regarding the carbon composition in the MPL, the mixture of CB 50% and AB 50% provided a suitable porosity and a reasonable number of surface nucleation sites for the growth of aligned Pt NWs to achieve a high power performance PtNW GDE. The higher CB amount made Pt NWs to grow into the inner pore surface between the active CB spheres while the higher AB content resulted in agglomerates and sparse distribution of Pt NWs owing to the inert surface properties. Furthermore, the PTFE amount within the MPL needs to be kept as low as possible to enable effective nucleation sites on the surface while can still prevent water flooding during fuel cell operation. The understanding obtained here can potentially provide reference for the design and development of fuel cell electrodes with other advanced nanostructures.

Supporting Information

Supporting Information is available from Elsevier or from the author.

Acknowledgements

Y. X. Lu is supported by a joint Li Siguang Scholarship from the University of Birmingham (UOB) and the China Scholarship Council (CSC). TEM analysis was performed at Leeds EPSRC Nanoscience and Nanotechnology Research Equipment Facility funded by EPSRC Grant EP/F056311/1 and the University of Leeds (LENNF).

References

[1] S.K. Kamarudin, N. Hashim, Materials, morphologies and structures of MEAs in DMFCs, Renew Sust Energ Rev, 16 (2012) 2494-2515.

[2] A. El-Kharouf, T.J. Mason, D.J.L. Brett, B.G. Pollet, Ex-situ characterisation of gas diffusion layers for proton exchange membrane fuel cells, J Power Sources, 218 (2012) 393-404.

[3] S. Park, J.W. Lee, B.N. Popov, A review of gas diffusion layer in PEM fuel cells: Materials and designs, International Journal of Hydrogen Energy, 37 (2012) 5850-5865.

[4] C. Chan, N. Zamel, X.G. Li, J. Shen, Experimental measurement of effective diffusion coefficient of gas diffusion layer/microporous layer in PEM fuel cells, Electrochimica Acta, 65 (2012) 13-21.

[5] J.S. Preston, R.S. Fu, U. Pasaogullari, D.S. Hussey, D.L. Jacobson, Consideration of the Role of Micro-Porous Layer on Liquid Water Distribution in Polymer Electrolyte Fuel Cells, Journal of the Electrochemical Society, 158 (2011) B239-B246.

[6] G.S. Hwang, A.Z. Weber, Effective-Diffusivity Measurement of Partially-Saturated Fuel-Cell Gas-Diffusion Layers, Journal of the Electrochemical Society, 159 (2012) F683-F692.

[7] T. Kitahara, H. Nakajima, K. Mori, Hydrophilic and hydrophobic double microporous layer coated gas diffusion layer for enhancing performance of polymer electrolyte fuel cells under no-humidification at the cathode, J Power Sources, 199 (2012) 29-36.

[8] C. Santoro, A. Agrios, U. Pasaogullari, B.K. Li, Effects of gas diffusion layer (GDL) and micro porous layer (MPL) on cathode performance in microbial fuel cells (MFCs), International Journal of Hydrogen Energy, 36 (2011) 13096-13104.

[9] H.H. Chen, M.H. Chang, Effect of cathode microporous layer composition on proton exchange membrane fuel cell performance under different air inlet relative humidity, J Power Sources, 232 (2013) 306-309.

[10] A. Rofaiel, J.S. Ellis, P.R. Challa, A. Bazylak, Heterogeneous through-plane distributions of polytetrafluoroethylene in polymer electrolyte membrane fuel cell gas diffusion layers, J Power Sources, 201 (2012) 219-225.

[11] A. Arvay, E. Yli-Rantala, C.H. Liu, X.H. Peng, P. Koski, L. Cindrella, P. Kauranen, P.M. Wilde, A.M. Kannan, Characterization techniques for gas diffusion layers for proton exchange membrane fuel cells - A review, J Power Sources, 213 (2012) 317-337.

[12] N. Parikh, J.S. Allen, R.S. Yassar, Microstructure of Gas Diffusion Layers for PEM Fuel Cells, Fuel Cells, 12 (2012) 382-390.

[13] E. Passalacqua, G. Squadrito, F. Lufrano, A. Patti, L. Giorgi, Effects of the diffusion layer characteristics on the performance of polymer electrolyte fuel cell electrodes, Journal of Applied Electrochemistry, 31 (2001) 449-454.

[14] Y. Xiao, M.L. Dou, J.L. Yuan, M. Hou, W. Song, B. Sunden, Fabrication Process Simulation of a PEM Fuel Cell Catalyst Layer and Its Microscopic Structure Characteristics, Journal of the Electrochemical Society, 159 (2012) B308-B314.

[15] T. Kitahara, H. Nakajima, K. Okamura, <Gas diffusion layers >, J Power Sources, 283 (2015) 115-124.

[16] Z. Fishman, A. Bazylak, Heterogeneous Through-Plane Porosity Distributions for Treated PEMFC GDLs I. PTFE Effect, J Electrochem Soc, 158 (2011) B841-B845.

[17] C. Lau, E.R. Adkins, R.P. Ramasamy, H.R. Luckarift, G.R. Johnson, P. Atanassov, Design of Carbon Nanotube-Based Gas-Diffusion Cathode for O2 Reduction by Multicopper Oxidases, Advanced Energy Materials, 2 (2012) 162-168.

[18] Y.X. Lu, S.F. Du, R. Steinberger-Wilckens, One-dimensional nanostructured electrocatalysts for polymer electrolyte membrane fuel cells—A review, Appl Catal B-Environ, 199 (2016) 292-314..

[19] B. Millington, S.F. Du, B.G. Pollet, The effect of materials on proton exchange membrane fuel cell electrode performance, J Power Sources, 196 (2011) 9013-9017.

[20] H.R. Jhong, F.R. Brushett, P.J.A. Kenis, The Effects of Catalyst Layer Deposition Methodology on Electrode Performance, Advanced Energy Materials, 3 (2013) 589-599.

[21] L. Wang, S.G. Advani, A.K. Prasad, Membrane Electrode Assembly with Enhanced Membrane/Electrode Interface for Proton Exchange Membrane Fuel Cells, J Phys Chem C, 117 (2013) 945-948.

[22] B. Millington, V. Whipple, B.G. Pollet, A novel method for preparing proton exchange membrane fuel cell electrodes by the ultrasonic-spray technique, J Power Sources, 196 (2011) 8500-8508.

[23] D.S. Hwang, C.H. Park, S.C. Yi, Y.M. Lee, Optimal catalyst layer structure of polymer electrolyte membrane fuel cell, International Journal of Hydrogen Energy, 36 (2011) 9876-9885.

[24] C. Bois, A. Blayo, D. Chaussy, R. Vincent, A.G. Mercier, C. Nayoze, Catalyst Layers for PEMFC Manufactured by Flexography Printing Process: Performances and Structure, Fuel Cells, 12 (2012) 199-211.

[25] S.F. Du, A Facile Route for Polymer Electrolyte Membrane Fuel Cell Electrodes with in situ Grown Pt Nanowires, J Power Sources, 195 (2010) 289-292.

[26] S.F. Du, B.G. Pollee, Catalyst loading for Pt-nanowire thin film electrodes in PEFCs, Int J Hydrogen Energ, 37 (2012) 17892-17898.

[27] S.F. Du, B. Millington, B.G. Pollet, The effect of Nafion ionomer loading coated on gas diffusion electrodes with in-situ grown Pt nanowires and their durability in proton exchange membrane fuel cells, International Journal of Hydrogen Energy, 36 (2011) 4386-4393.

[28] S.F. Du, K.J. Lin, S.K. Malladi, Y.X. Lu, S.H. Sun, Q. Xu, R. Steinberger-Wilckens, H.S. Dong, Plasma nitriding induced growth of Pt-nanowire arrays as high performance electrocatalysts for fuel cells, Scientific Reports, 4 (2014).

[29] S. Park, J.W. Lee, B.N. Popov, Effect of carbon loading in microporous layer on PEM fuel cell performance, J Power Sources, 163 (2006) 357-363.

[30] M.Y. Jing, L.H. Jiang, S.L. Wang, F.N. Jing, G.Q. Sun, Application of FTIR in direct methanol fuel cells - Quantitative analysis of PTFE in gas diffusion layers, International Journal of Hydrogen Energy, 38 (2013) 7957-7963.

[31] S. Park, J.W. Lee, B.N. Popov, Effect of PTFE content in microporous layer on water management in PEM fuel cells, J Power Sources, 177 (2008) 457-463.

[32] Y.X. Lu, S.F. Du, R. Steinberger-Wilckens, Temperature-controlled growth of single-crystal Pt nanowire arrays for high performance catalyst electrodes in polymer electrolyte fuel cells, Appl Catal B-Environ, 164 (2015) 389-395.

[33] Y.X. Lu, S.F. Du, R. Steinberger-Wilckens, Three-dimensional catalyst electrodes based on PtPd nanodendrites for oxygen reduction reaction in PEFC applications, Appl Catal B-Environ, 187 (2016) 108-114.

[34] T.J. Schmidt, H.A. Gasteiger, G.D. Stab, P.M. Urban, D.M. Kolb, R.J. Behm, Characterization of high-surface area electrocatalysts using a rotating disk electrode configuration, J Electrochem Soc, 145 (1998) 2354-2358.

[35] N. Zamel, J. Becker, A. Wiegmann, Estimating the thermal conductivity and diffusion coefficient of the microporous layer of polymer electrolyte membrane fuel cells, J Power Sources, 207 (2012) 70-80.

[36] Y. Xiao, M. Dou, J. Yuan, M. Hou, W. Song, B. Sundén, Fabrication Process Simulation of a PEM Fuel Cell Catalyst Layer and Its Microscopic Structure Characteristics, J Electrochem Soc, 159 (2012) B308-B314.

[37] T. Kitahara, H. Nakajima, K. Okamura, Gas diffusion layers coated with a microporous layer containing hydrophilic carbon nanotubes for performance enhancement of polymer electrolyte fuel cells under both low and high humidity conditions, J. Power Sources, 283 (2015) 115-124.

[38] H.Y. Du, C.H. Wang, H.C. Hsu, S.T. Chang, S.C. Yen, L.C. Chen, B. Viswanathan, K.H. Chen, High performance of catalysts supported by directly grown PTFE-free micro-porous

CNT layer in a proton exchange membrane fuel cell, Journal of Materials Chemistry, 21 (2011) 2512-2516.

Figure and table captions

Table 1. Information of the PTFE loading in the standard and self-painted GDLs.

Fig. 1. Optical microscopy images of (a) 35BA substrate and the GDLs with self-painted MPLs at the Vulcan XC-72R CB loading of (b) 1, (c) 3, (d) 4, (e) 4.48 and (f) 5 mg cm^{-2}.

Fig. 2. (a) Polarisation and power density curves, and (b) the trend of the current density at 0.6 V and the maximum power density for Pt NWs GDEs with different CB loadings in the painted MPLs. (20% PTFE in MPLs based on the total MPL weight). Measurements were taken at T_{cell}=70 ^{o}C with fully humidified H_2 and air at 2 barg (stoichiometry s=1.3/2.4).

Fig. 3. SEM images at different magnifications for Pt NWs grown on the self-painted MPL with carbon loading of (a-d) 1 mg cm^{-2} (e) 4, (c) 5 mg cm^{-2} (20% PTFE in MPLs based on the total MPL weight). EIS measured at (g) 0.05, (h) 0.5 and (i) 1.0 A cm^{-2} for Pt NWs GDEs with different CB loadings in the painted MPLs. (20% PTFE in MPLs based on the total MPL weight). Measurements were taken at T_{cell}=70 ^{o}C with fully humidified H_2 and air at 2 barg (stoichiometry s=1.3/2.4).

Fig. 4. (a) Polarisation and power density curves, and (b) the trend of the current density at 0.6 V and the maximum power density for Pt NWs GDEs with different carbon compositions in the painted MPLs. EIS measured at (c) 0.05, (d) 0.5 and (e) 1.0 A cm^{-2} for Pt NWs GDEs with different carbon compositions in the painted MPLs. Measurements were taken at T_{cell}=70 ^{o}C with fully humidified H_2 and air at 2 barg (stoichiometry s=1.3/2.4). SEM images for Pt NWs grown on the self-painted MPL with (f) pure AB, (g) CB 50% + AB 50%, (h) pure CB. (Carbon loading is 4 mg cm^{-2}, PTFE is 20%).

Fig. 5. Polarisation and power density curves of Pt NWs GDEs with different PTFE loadings in self-painted MPLs. Measurements were taken at T_{cell}=70 ^{o}C with fully humidified H_2 and air at 2 barg (stoichiometry s=1.3/2.4).

Fig. 6. EIS measured at (a) 0.05, (b) 0.5 and (c) 1.0 A cm^{-2} for Pt NWs GDEs with different PTFE loadings in the self-painted MPLs. SEM images of Pt NWs GDEs with (d) 5%, (e) 20% and (f) 40% PTFE amount in the self-painted MPLs. Measurements were taken at T_{cell}=70 ^{o}C with fully humidified H_2 and air at 2 barg (stoichiometry s=1.3/2.4).

Fig. 7. (a) Cathode CVs and (b) summary of ECSAs for the Pt NWs GDEs with different PTFE loadings in the MPLs. Measurements were taken at T_{cell}=70 ^{o}C with fully humidified H_2 and N_2 at 2 barg (stoichiometry s=1.3/2.4).

Fig. 8. Continuous operation test at 0.6 V for Pt NWs GDEs with painted MPLs at the low, medium and high PTFE amounts. Measurements were taken at T_{cell}=70 ^{o}C with fully humidified H_2 and air at 2 barg (stoichiometry s=1.3/2.4).

Fig. 9. Comparison of the cathode polarization curves of the in-situ growth of Pt NWs GDEs on Freudenberg H2315 I6 GDL carbon paper (Pt loading 0.4 mg cm^{-2}), E-TEK ELAT® GDEs LT120EW (Pt loading 0.5 mg cm^{-2}), Pt/C (20 wt%) nanoparticle GDEs, and the optimized in-situ growth Pt NWs GDEs in this work.

Table 1. Information of the PTFE loading in the standard and self-painted GDLs.

Type	GDL	PTFE loading in the substrate (%)	PTFE loading in the MPL (%)
Standard	35BA	5	No MPL
	35BC	5	20
	35CC	10	20
	35DC	20	20
Self-painted	35BA+MPL1	5	5
	35BA+MPL2	5	10
	35BA+MPL3	5	15
	35BA+MPL4	5	20
	35BA+MPL5	5	25
	35BA+MPL6	5	30
	35BA+MPL7	5	40

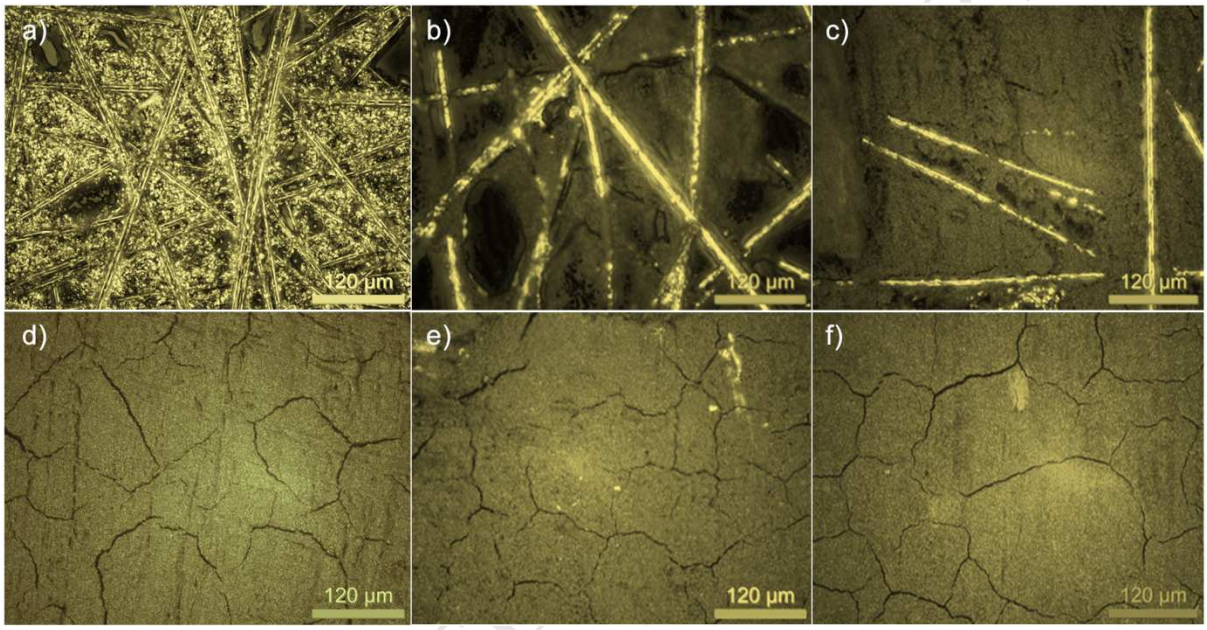

Fig. 1. Optical microscopy images of (a) 35BA substrate and the GDLs with self-painted MPLs at the Vulcan XC-72R CB loading of (b) 1, (c) 3, (d) 4, (e) 4.48 and (f) 5 mg cm^{-2}.

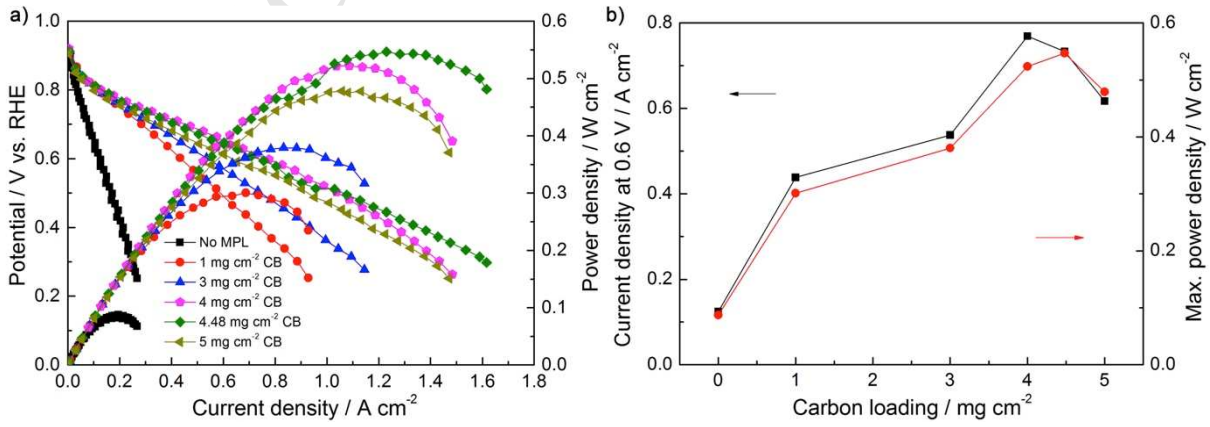

Fig. 2. (a) Polarisation and power density curves, and (b) the trend of the current density at 0.6 V and the maximum power density for Pt NWs GDEs with different CB loadings in the painted MPLs. (20% PTFE in MPLs based on the total MPL weight). Measurements were taken at T_{cell}=70 ^{o}C with fully humidified H_2 and air at 2 barg (stoichiometry s=1.3/2.4).

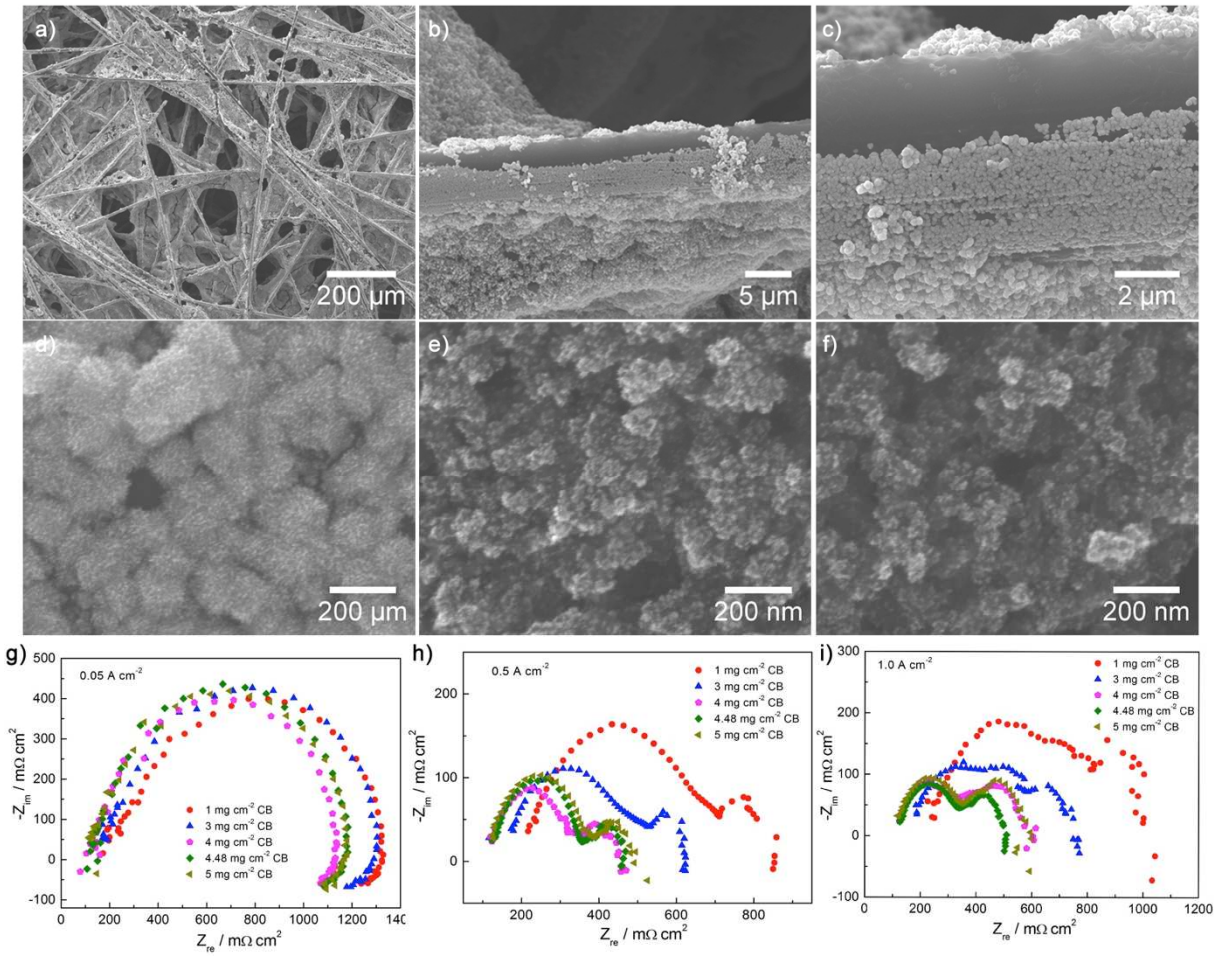

Fig. 3. SEM images at different magnifications for Pt NWs grown on the self-painted MPL with carbon loading of (a-d) 1 mg cm^{-2} (e) 4, (c) 5 mg cm^{-2} (20% PTFE in MPLs based on the total MPL weight). EIS measured at (g) 0.05, (h) 0.5 and (i) 1.0 A cm^{-2} for Pt NWs GDEs with different CB loadings in the painted MPLs. (20% PTFE in MPLs based on the total MPL weight). Measurements were taken at T_{cell}=70 ^{o}C with fully humidified H_2 and air at 2 barg (stoichiometry s=1.3/2.4).

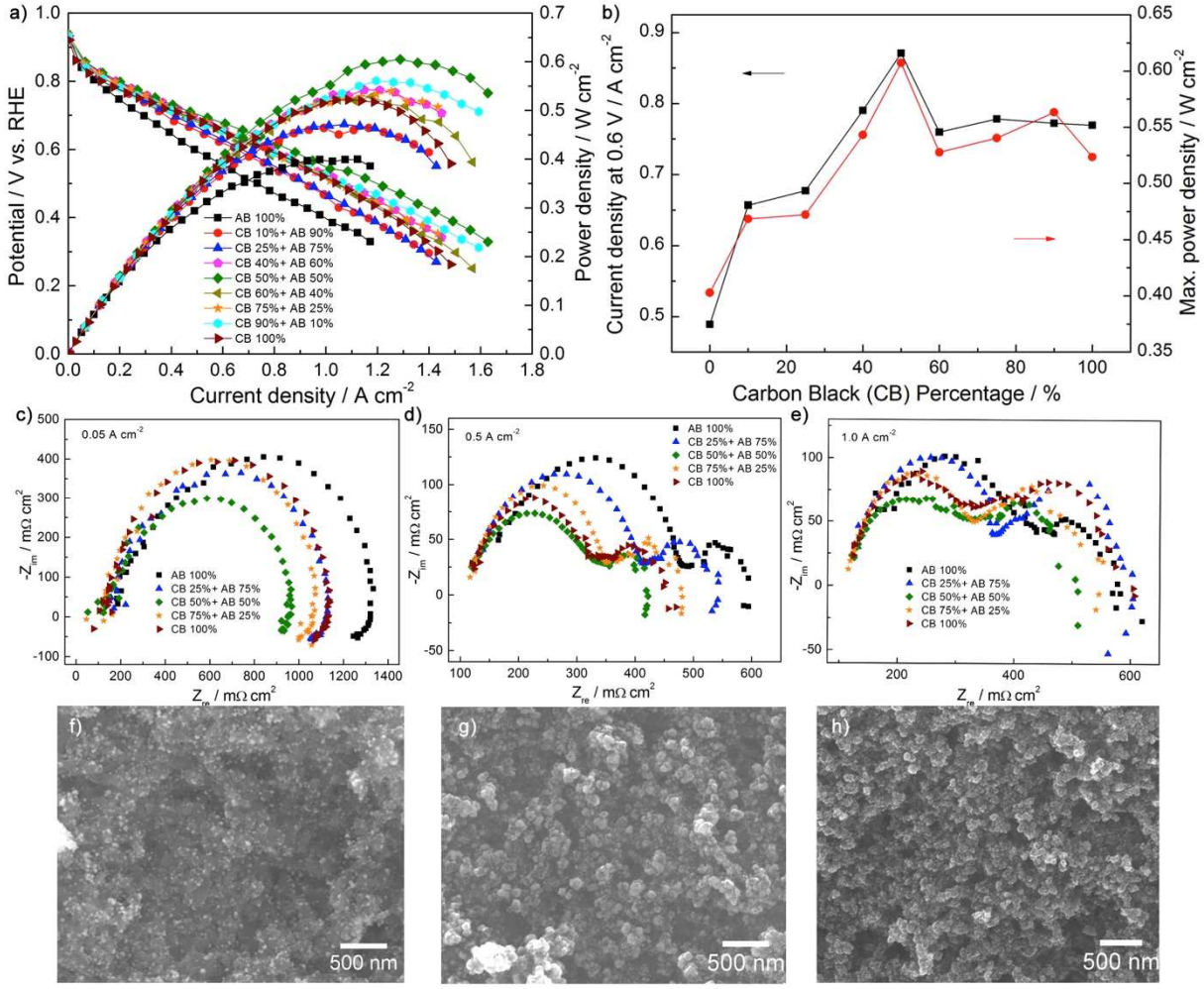

Fig. 4. (a) Polarisation and power density curves, and (b) the trend of the current density at 0.6 V and the maximum power density for Pt NWs GDEs with different carbon compositions in the painted MPLs. EIS measured at (c) 0.05, (d) 0.5 and (e) 1.0 A cm^{-2} for Pt NWs GDEs with different carbon compositions in the painted MPLs. Measurements were taken at T_{cell}=70 ^{o}C with fully humidified H_2 and air at 2 barg (stoichiometry s=1.3/2.4). SEM images for Pt NWs grown on the self-painted MPL with (f) pure AB, (g) CB 50% + AB 50%, (h) pure CB. (Carbon loading is 4 mg cm^{-2}, PTFE is 20%).

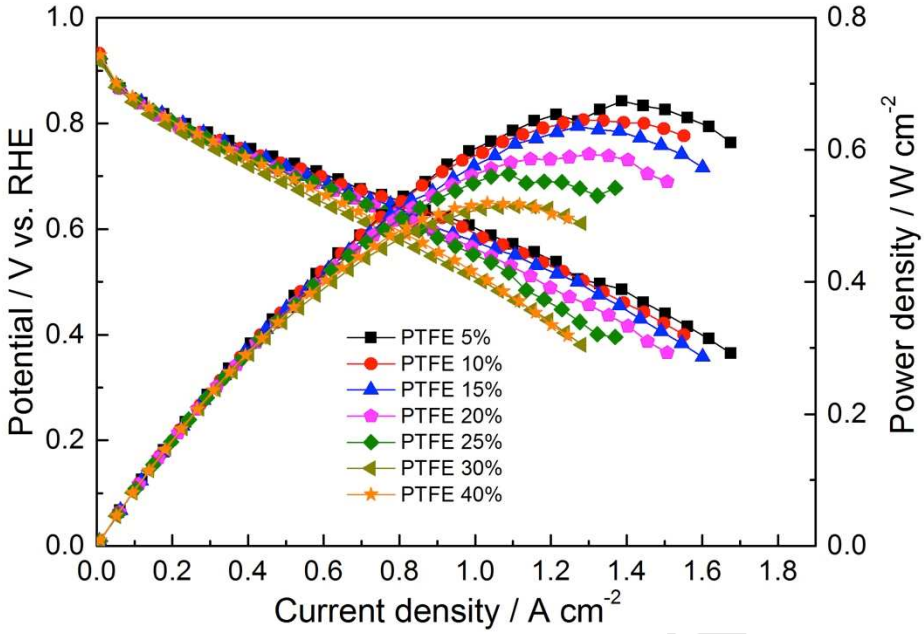

Fig. 5. Polarisation and power density curves of Pt NWs GDEs with different PTFE loadings in self-painted MPLs. Measurements were taken at T_{cell}=70 °C with fully humidified H_2 and air at 2 barg (stoichiometry s=1.3/2.4).

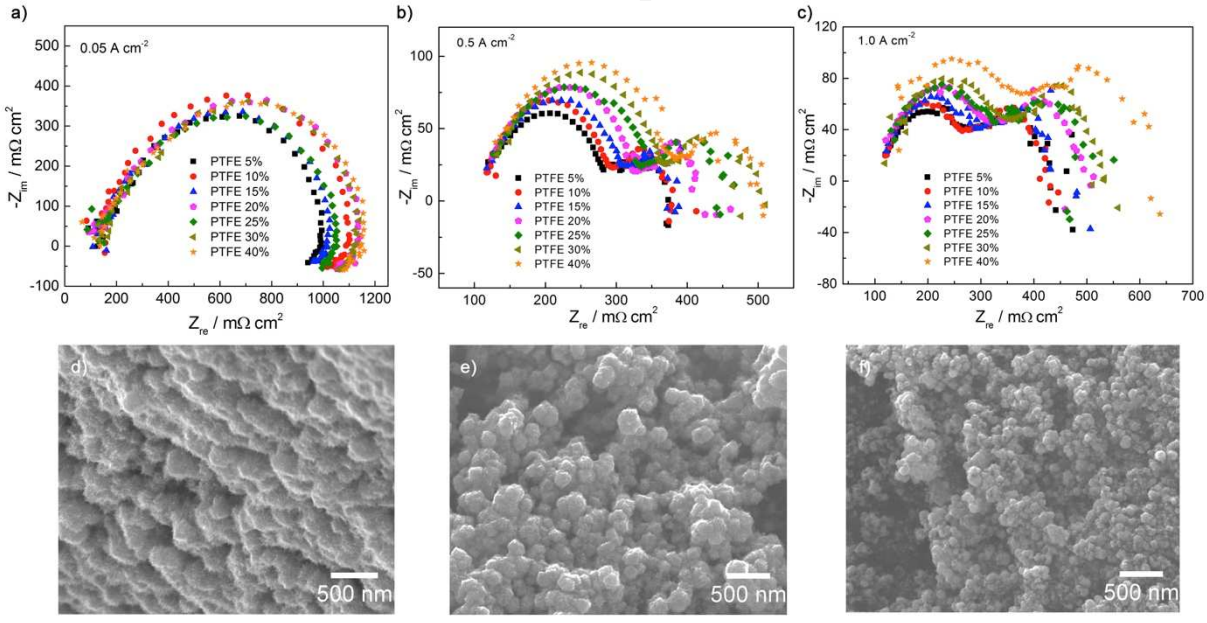

Fig. 6. EIS measured at (a) 0.05, (b) 0.5 and (c) 1.0 A cm^{-2} for Pt NWs GDEs with different PTFE loadings in the self-painted MPLs. SEM images of Pt NWs GDEs with (d) 5%, (e) 20% and (f) 40% PTFE amount in the self-painted MPLs. Measurements were taken at T_{cell}=70 °C with fully humidified H_2 and air at 2 barg (stoichiometry s=1.3/2.4).

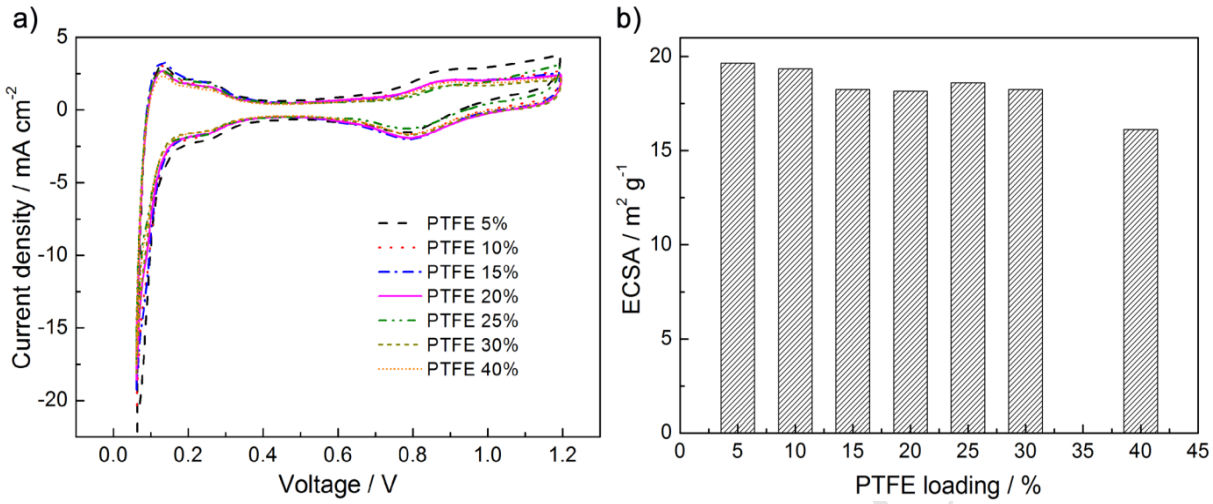

Fig. 7. (a) Cathode CVs and (b) summary of ECSAs for the Pt NWs GDEs with different PTFE loadings in the MPLs. Measurements were taken at T_{cell}=70 ^{o}C with fully humidified H_2 and N_2 at 2 barg (stoichiometry s=1.3/2.4).

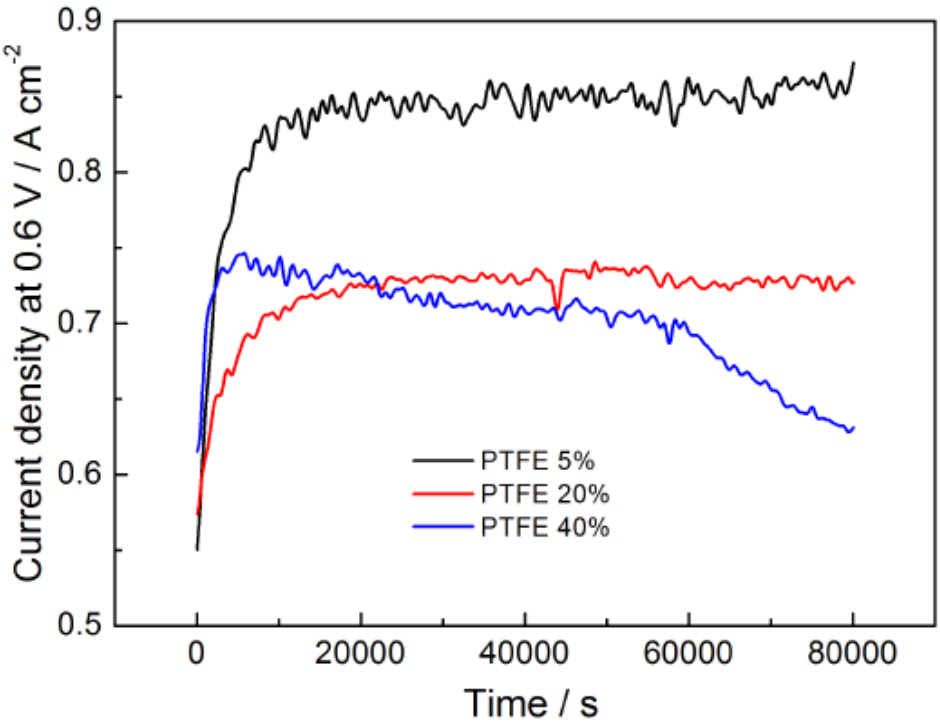

Fig. 8. Continuous operation test at 0.6 V for Pt NWs GDEs with painted MPLs at the low, medium and high PTFE amounts. Measurements were taken at T_{cell}=70 ^{o}C with fully humidified H_2 and air at 2 barg (stoichiometry s=1.3/2.4).

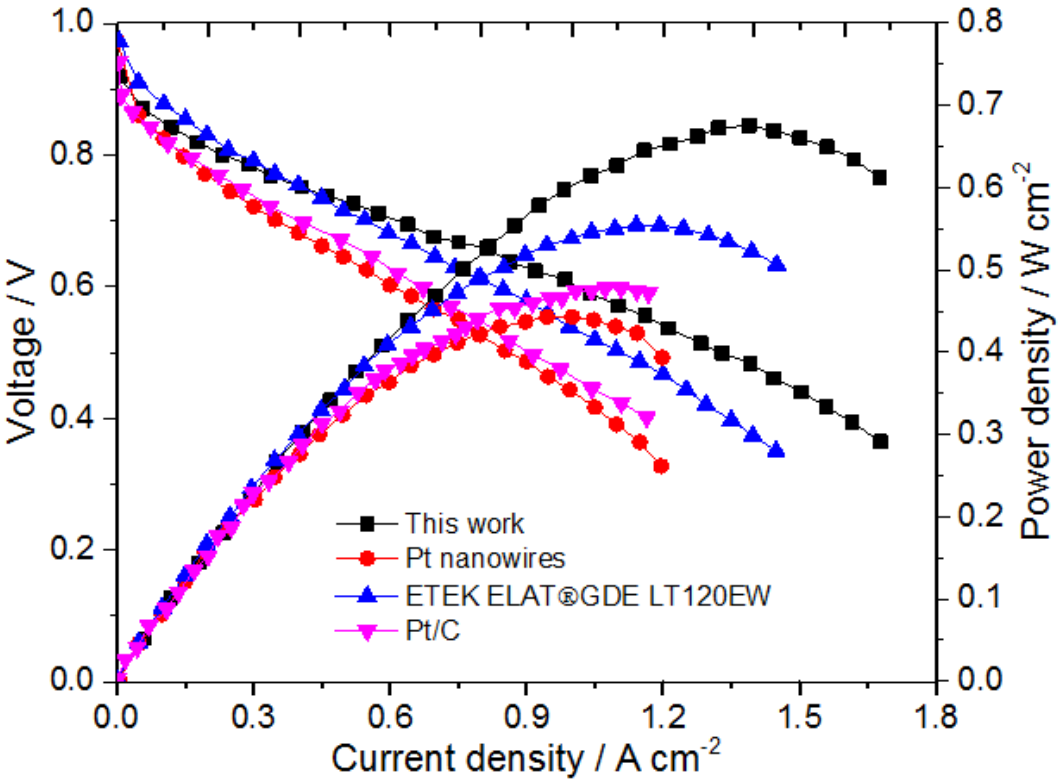

Fig. 9. Comparison of the cathode polarization curves of the in-situ growth of Pt NWs GDEs on Freudenberg H2315 I6 GDL carbon paper (Pt loading 0.4 mg cm^{-2}), E-TEK ELAT® GDEs LT120EW (Pt loading 0.5 mg cm^{-2}), Pt/C (20 wt%) nanoparticle GDEs, and the optimized in-situ growth Pt NWs GDEs in this work.